JOURNAL OF MATERIALS SCIENCE **40** (2005) 1599–1609

# Predicting dendrite arm spacing and their effect on microporosity formation in directionally solidified Al-Cu alloy

M. L. N. M. MELO*
*PPGECM, São Francisco University (USF), Itatiba-SP, Brazil*
*E-mail: mirian.melo@saofrancisco.edu.br*

E. M. S. RIZZO
*Department of Materials and Metallurgical Engineering, CEFETES, Vitória/ES, Brazil*

R. G. SANTOS
*Department of Materials Engineering, State University in Campinas (UNICAMP) C.P. 6122, Campinas-SP, Brazil*

In the case of metallic alloys, which present dendritic structure, the mechanical properties of foundry products depend on primary and secondary arm spacing. For the prediction of microporosities it is necessary to characterize precisely the dendritic structure formed during solidification, to calculate the permeability and also to estimate the radius of the gas bubble to determine the pressure due to gas/metal surface tension. Therefore, it is important in a computational simulation of the solidification processes to use reliable equations to correlate the calculated thermal parameters with primary and secondary dendrite arm spacing. This study presents a numerical and experimental analysis of some models to predict the primary and secondary arm spacing as a function of thermal parameters. Comparison between the numerical and experimental results for Al 4.5 wt% Cu alloy allowed the selection of adequate equations to predict the dendritic spacing during unidirectional solidification. 

## 1. Introduction

Microporosity may be found after solidification, specially in alloys which freeze over a temperature range presenting a dendritic structure, and influences directly the mechanical properties of castings [1–3]. The dendritic structure is characterized by primary and secondary dendrite arm spacings. Microporosity may occur during solidification of castings either due to rejection of gas from the liquid metal or to the inability of liquid metal to feed through interdendritic channels in order to compensate for the shrinkage [4–17]. Analysis of microporosity formation is complex because it depends on interdendritic fluid flow and it is affected by parameters such as alloy composition, gas content, casting geometry and thermal properties of mold, which directly influence the solidification process. As the fluid flow in the interdendritic channels depends on the primary and secondary dendrite arm spacing, it is important to know the variation of these parameters during the solidification process to analyze microporosity formation.Formation of dendritic structure has been studied during the last decades and different approaches and equations have been used to estimate primary and secondary arms spacings. The interdendritic spacings [18–35] and parameters related to pore formation, such as solid fraction [18, 26, 30, 36, 37], permeability [38–45] and evolution of dissolved gases [1, 5–17, 46–48] have been used to predict the position and size of microporosity [5, 7, 8, 11, 14–16, 38, 45–48].

The aim of the present work is to analyze the application of some models frequently used to estimate the primary and secondary arms spacings, to predict the microstructure formation in an Al 4.5 wt% Cu alloy, and to apply a numerical model to evaluate the dendritic arm spacing influence on the prediction of microporosity formation.

## 2. Numerical model

A numerical simulation to predict the microstructure and the microporosity formation during solidification must be able to describe precisely the evolution of *solid* and *liquid* isotherms, temperature variation in the casting and in the mold and the primary and secondary dendritic arms spacings. On the other hand, it is necessary to know the pressure drop in the interdendritic channels, which depend on the permeability of the

*Author to whom all correspondence should be addressed.

dendritic array, and of the gas content in the liquid and its solubility in the liquid and solid phases.

## 2.1. Modeling

Considering that solidification of alloys is primarily governed by heat diffusion, the basic continuity equation at macroscopic scale is the equation of conservation of energy given by [20]:

$$\rho \cdot c_p \cdot \frac{\partial T}{\partial t} = \nabla \cdot (k \cdot \nabla T) + Q \tag{1}$$

where $\rho$ is the density of solid metal, $c_p$ is the specific heat of solid metal, $k$ is the thermal conductivity of solid metal, $Q$ is the heat liberated during solidification, $T$ is the temperature and $t$ is the time.

The heat liberated during solidification is taken into account applying the enthalpy model. The fraction of solid as function of temperature is determined using the Scheil equation [21] and the curve of variation of enthalpy versus temperature can be calculated.

Considering variable thermophysical properties and variable heat transfer coefficient in the metal/mold interface and following a suitable discretization of the metal/mould system, the differential equations, considering unidirectional solidification, are solved using finite difference method. The temperatures are determined from the values of enthalpy, using the curve of variation of enthalpy versus temperature, and the positions of the solidus and liquidus isotherms during solidification are obtained. From these parameters it is possible to calculate the rate of dendrites tip movement, the local solidification time and thermal gradients ahead of dendrite tips and then predict the variation of dendrite arms spacing during solidification. More details of the numerical model have been presented in a previous paper [17].

## 2.2. Microstructural prediction

For prediction of the interdendritic spacing, there are basically two types of models: theoretical, based on thermal parameters and on geometrical relations and empirical, based exclusively on experimental results.

Theoretical analysis of the primary dendrite arm spacing has been carried out since 1960 [19]. Models to determine the primary spacing have been proposed, considering the advance velocity of dendrite tip ($V_{liq}$), interface temperature gradient in the *liquidus* front ($G_{liq}$), and the composition of the alloy. For dendritic growth, when the advance velocity of dendrite tip ($V_{liq}$) is high related to the velocity of transition from cellular to dendritic structure ($V_{cd}$), Hunt [22] applying a mass balance and assuming that the region close to the dendrite tip can be considered approximated spherical, proposed the following equation for primary interdendritic arm spacing:

$$\lambda_1 = 2.83 \sqrt[4]{\frac{D_{liq}\Gamma k \Delta T_0}{V_{liq} G_{liq}^2}} \tag{1}$$

where $D_{liq}$ is the diffusion coefficient in the liquid in m/s$^2$, $\Gamma$ is the Gibbs-Thompson coefficient in mK, $k$ is the partition coefficient, $G_{liq}$ is liquid temperature gradient in °C/m, $V_{liq}$ is the advance velocity of the *liquidus* isotherm or of the dendrite tip in m/s and $\Delta T_0$ is the liquidus-solidus range in °C given by:

$$\Delta T_0 = \frac{-mC_0(1-k)}{k} \tag{2}$$

where $C_0$ is the initial concentration of solute of the alloy in wt% and $m$ is the *liquidus* slope in °C/wt%.

Another theoretical model to characterize interdendritic spacing was proposed by Kurz and Fisher [18] assuming that the tip radius of the dendrite, and the length of the interdendritic liquid zone can determine the primary spacing. They assumed that the mean cross section of the trunk and branches of the dendrite can be considered as an ellipsoid and proposed that for high interface rate, the primary dendritic spacing become:

$$\lambda_1 = 4.3 \sqrt[4]{\frac{\Delta T_0 D_{liq}\Gamma}{k V_{liq} G_{liq}^2}} \tag{3}$$

Trivedi [23] considering the interference of the neighboring dendritic branches and assuming a spherical approximation for the interface, in the case of dendritic growth, with low values for the $G_{liq}/V_{liq}$ relation, proposed that the equation for primary spacing could be written in the following manner:

$$\lambda_1 = 6 \sqrt[4]{\frac{\Delta T_0 D_{liq}\Gamma}{k V_{liq} G_{liq}^2}} \tag{4}$$

Geying and Lixin [24] based on Hunt's model [22] and on Trivedi's equation [23] proposed the following equation, to calculate primary spacing for high interface velocity:

$$\lambda_1 = 1.34 \sqrt{\left(\frac{1}{2}(l+1)(l+2)\right)} \sqrt[4]{\frac{\Delta T_0 D_{liq}\Gamma k}{V_{liq} G_{liq}^2}} \tag{5}$$

where, for dendritic growth Trivedi proposed $l = 6$.

Empirical models were proposed by observing that primary interdendritic spacing decreases with the increase in thermal gradient ($G_{liq}$) and/or growth velocity ($V_{liq}$) determined in the *liquidus* isotherm or dendrite tip. Young and Kirkwood [25] proposed, from experimental data for the Al-Cu alloy with 4.4 and 6.0 wt% Cu, the following equation:

$$\lambda_1 = 3050 G_{liq}^{-0.5} V_{liq}^{-0.36} \tag{6}$$

where $\lambda_1$ is in $\mu$m, $V_{liq}$ in $\mu$m/s and $G_{liq}$ in °C/mm.

McCartney e Hunt [32] utilizing experimental data for Al 6 wt% Cu obtained:

$$\lambda_1 = 359 G_{liq}^{-0.474} V_{liq}^{-0.31} \tag{7}$$

where $\lambda_1$ is in $\mu$m, $V_{liq}$ in mm/s and $G_{liq}$ in K/mm.

After being established primary spacing does not vary, which does not occur with secondary spacing due to the coarsening effect [18]. Coarsening of the dendrite secondary arms occurs through the mechanism of refusion of the thin secondary arms and the thickening of the thicker arms [18, 26].

Theoretical models to predict secondary arm ($\lambda_2$) have also been proposed, considering local solidification time ($t_{local}$) and are based on two basic concepts [27]: Fick's law and the Gibbs-Thompson equation, which are used to develop idealized thickening models.The basic difference between the models is the condition adopted on refusion of the secondary branches. For example, Feurer [28] considered thickening as being a consequence of refusion of the thin lateral branches and proposed the following equation:

$$\lambda_2 = 5.5 \cdot (M t_{local})^{1/3} \tag{8}$$

where $M$ is a coarsening parameter that represents the influence of the type of alloy and initial composition in the value of secondary arm, and is given by the following equation:

$$M = \frac{2\sigma_{sl} D_{liq} T_{liq} \ln\left(\frac{C_{liq}}{C_0}\right)}{H_f (1-k)\, m(C_{liq} - C_0)} \tag{9}$$

where $\sigma_{sl}$ is solid/liquid interfacial energy in J/m$^2$, $C_{liq}$ is the final concentration of the liquid in wt%, which is sometimes equal to $C_{eut}$ and $H_f$ volumetric latent heat of fusion in J/m$^3$.

Kirkwood [29]proposed a theoretical model for coarsening, based on the refusion of thin branches, beginning at the tip and dislocating towards the root, and proposed the following equation for secondary spacing:

$$\lambda_2 = \left(\frac{128\Gamma D_{liq} \ln\left(\frac{C_{liq}}{C_0}\right) t_{local}}{(1-k) m_{liq}(C_0 - C_{liq})}\right)^{1/3} \cong 5\left(\frac{\Gamma D_{liq} \ln\left(\frac{C_{liq}}{C_0}\right) t_{local}}{(1-k) m_{liq}(C_0 - C_{liq})}\right)^{1/3} \tag{10}$$

Empirical models for the secondary dendrites arm spacing, based exclusively on experimental results, have also been carried out. An example of empirical models for the prediction of secondary arm is the Bower *et al.* model [30] proposed for the Al 4.5 wt% Cu alloy:

$$\lambda_2 = 7.5 \times 10^{-6} (t_{local})^{0.39} \tag{11}$$

Jones *et al.* [34] proposed a different model based on cooling rate ($R$) given by:

$$\lambda_2 = 50(R)^{-1/3} = 50\left(\frac{T_{liq} - T_{sol}}{t_{local}}\right)^{-1/3} \tag{12}$$

## 2.3. Prediction of microporosity formation

In the last decades, researches have been developed on many aspects related to microporosities formation. But, there are already discussions on whether the pore formation in the cast metal is caused primarily by contraction, dissolved gases or by a combination of both. While some authors [50–53] consider only metal contraction, others [55, 56] affirm that the first traces of gas are necessary to form microporosities, and that it does not occur in a completely gas free casting. Others [1, 4, 5, 16, 54, 57, 58] suggest that simultaneous occurrence of contraction and gas evolution is essential to form microporosities.

Favorable conditions for microporosity formation are inefficient liquid feed; difficulty in interdendritic flow, low energy for pore nucleation; low pressure acting on the liquid metal; surface tension; high gas content and low gas solubility in the solid phase [56]. These conditions for porosity formation are expressed in terms of pressures and predict the thermodynamic condition for porosity formation in castings by the equation [1, 2, 4–9, 12, 13, 16, 26, 39, 57]:

$$P_G + \Delta P \geq P_A + P_M + P_\sigma \tag{13}$$

where $P_G$ is the pressure of dissolved gases in the melt, $\Delta P$ is the pressure drop in interdendritic channels, $P_A$ is the atmospheric pressure, $P_M$ is the metalostatic pressure and $P_\sigma$ is the pressure necessary to overcome surface tension.

During solidification, the rejection of gas at the solid/liquid interface leads to an increased gas concentration in the liquid. If this concentration reaches a critical value, based on the net solubility of gas in the liquid, then pores can nucleate and grow [5, 7–9, 16].

In the case of aluminum alloys, hydrogen is the gas of highest interest [12, 49, 58]and the equation to determine gas pressure assumes that there is a complete diffusion of hydrogen in the liquid [4, 7, 55]. Diatomic gases generally dissociate when they are dissolved in metals. For diluted solutions, and assuming the behavior of an ideal gas, the Sievert's law can be applied [8, 9] and:

$$P_{gas} = 10^5 \cdot \left(\frac{H_{liq}}{S}\right)^2 \tag{14}$$

where $H_{liq}$ is weight percentage of gas (hydrogen) dissolved in the liquid and $S$ is the solubility in cm$^3$ per 100 g of alloy per atm$^{1/2}$.

As the solid and liquid phases coexist inside the mushy zone and the dendritic spacing is generally very small, it is reasonable to assume that the gas rejected by the solid phase diffuses entirely into the liquid phase before forming micropores. In this manner, it can be assumed that the initial quantity of gas in the solidifying alloy should be conserved and a balance of mass can be made [5, 16, 54, 55]:

$$H_0 = H_{sol} \cdot (1 - f_{liq}) + H_{liq} \cdot f_{liq} \tag{15}$$

where $H_0$ is the nominal concentration of gas dissolved in the liquid metal, $H_{sol}$ is amount of gas in the solid phase; $H_{liq}$ is amount of gas in the liquid phase and $f_{liq}$ is liquid fraction.

Usually a metal at high temperature can dissolve more gases, and the gas solubility in a molten metal is, in general, function of temperature. As the solubility of the solid phase is smaller, part of gas will be rejected from the growing dendrites into the interdendritic liquid during solidification, and can be determined by the equation [1, 4, 59, 60]:

$$\log S = \frac{-A}{T} + B \tag{16}$$

where $A$ and $B$ are parameters that depend only on concentration of solute in alloys, and $T$ is temperature in $K$. The solubility ($S$) should consider the rejection of solute in the interdendritic liquid [11]. For the Al-Cu alloys, using a regression analysis, the values of $A$ and $B$ given by Opie and Grant [11] are:

$$A = 2550 + 358.9C_{\mathrm{Cu}}^{1/2} - 54.48C_{\mathrm{Cu}} + 0.641C_{\mathrm{Cu}}^{3/2} \tag{17}$$

and

$$B = 2.620 + 0.3043C_{\mathrm{Cu}}^{1/2} - 0.08072C_{\mathrm{Cu}} + 0.0004484C_{\mathrm{Cu}}^{3/2} \tag{18}$$

with $C_{\mathrm{Cu}}$ as the wt pct of copper in the liquid.

To compensate metal contraction during solidification, there should be a flow of liquid metal into the interdendritic channels. The increase in roughness of the interdendritic channels, caused by the successive ramification of the dendritic arms, promotes a pressure drop inside the channel ($\Delta P$). Considering only the formation of porosity through contraction, pores are formed when the pressure drop at a point within the mushy zone is larger than the pressure acting at that point [1, 51, 61].

Since the interdendritic channels are quite small, the liquid metal that flows through them can be treated as a flow through a porous media. So the pressure drop inside the interdendritic channels was determined using Darcy's law [1, 4, 7, 16, 46, 55, 61, 62]. In the case of vertical directional solidification, with heat being removed through the lower part of the mold, the liquid metal flow is parallel to the primary dendritic branches. Therefore, pressure drop inside the channels, for a certain point within the mushy zone, in a certain instant, can be determined by the equation:

$$\Delta P = -\int_0^L \frac{V_{\mathrm{flux}} \cdot \mu \cdot g_{\mathrm{liq}}}{K} \mathrm{d}y \tag{19}$$

where $V_{\mathrm{flux}}$ is the velocity of the liquid metal flow in the y direction, in m/s, $\mu$ is the dynamic viscosity of the liquid metal in kg/m · s, $g_{\mathrm{liq}}$ is the volumetric liquid fraction; $K$ is the permeability in $\mathrm{m}^2$, $L$ is the length of the mushy zone, given by the distance between the positions of *liquidus* and *solidus* temperatures, at a certain moment.

To determine the pressure drop that occurs during the liquid flow in the interdendritic channel, it is necessary to calculate the permeability of the dendritic network. During solidification, a continuous variation is observed in the interdendritic primary and secondary spacing; therefore, permeability also varies during the solidification process. In another paper [17] a comparison is presented between different permeability models proposed by Flemings *et al.* [39], Poirier [4, 63], Santos [15, 65], Carman-Kozeny [5, 13, 39, 64] and Murakami [66]. The results indicated that the use of the equation proposed by Santos [15] becomes interesting, as it is an equation based on process parameters ($\lambda_1$,$\lambda_2$, $g_{\mathrm{liq}}$), and not on parameters arising from linear regressions with an interval of restricted validity. It is important to note that, while models in general consider constant tortuosity [8, 26, 38], this equation, proposed by Santos [15], considers a variation of the tortuosity with the liquid fraction. The equation to determine pressure drop (Equation 19) now becomes:

$$\Delta P = \int_0^L \frac{8\pi\left(\frac{\rho_{\mathrm{sol}}-\rho_{\mathrm{liq}}}{\rho_{\mathrm{sol}}}\right)V_{\mathrm{sol}}\mu}{\lambda_1^2 g_{\mathrm{liq}}}\left(1 + \sum_{n=1}^{3}\left(\frac{\lambda_2}{\lambda_1}\right)^{g_{\mathrm{liq}}^n}\right)\mathrm{d}y \tag{20}$$

where $\rho_{\mathrm{sol}}$ and $\rho_{\mathrm{liq}}$ are the densities of the solidus and liquidus phases respectively, and $V_{\mathrm{sol}}$ is the velocity of the liquid metal flow in the $y$ direction, in m/s.

Pressure caused by surface tension of the liquid/gas interface represents an initial resistance to the formation of the gas bubble, varying with many factors and nucleation mechanisms [67]. A bubble cannot be stabilized for a radius tending to zero because the pressure due to tension would tend to an infinite value. But there is a critical size of bubble, below which it is not able to survive and above which it tends to grow [2]. To calculate this pressure it is used the Laplace's equation, which relates the pressure difference along the interface with the surface tension and the principal curvature radii of this interface at the point considered [1, 2, 4, 5, 8, 9, 11, 12, 16, 49, 54, 67]. This equation is given by:

$$P_\sigma = \sigma_{\mathrm{lg}}\left(\frac{1}{r_1} + \frac{1}{r_2}\right) \cong \frac{\sigma_{\mathrm{lg}}}{r_{\mathrm{p}}} \tag{21}$$

where $\sigma_{\mathrm{lg}}$ is the surface tension of the liquid/gas interface, in $\mathrm{N/m}^2$, and $r_1$ and $r_2$ are the principal curvature radii of the pore, in m, which depend upon the volume of interdendritic space and its geometry and the contact angle at the junction between gas, solid and liquid.

Considering that the microsegregation of solute influences the solubility of the hydrogen for the Al-Cu alloys [68], the equation for surface tension is given by:

$$\sigma_{\mathrm{lg}} = 0.868 + 0.761 \times 10^{-3}C_{\mathrm{Cu,liq}} + 1.29 \times 10^{-5}C_{\mathrm{Cu,liq}} \tag{22}$$

where $C_{\mathrm{Cu,liq}}$ is concentration of copper, in the interdendritic liquid, in wt%, obtained through the Scheil [21] equation.

One of the problems for modeling microporosities formation is to predict the critical initial radius ($r_p$). To estimate initially this radius, it is necessary to characterize the dendritic structure of the alloy during solidification. For example, considering the dendritic structure formed, interdendritic microporosities can be located between primary spacings or between secondary branches.

Kubo and Pehlke [5], for an Al 4.5 wt% C alloy directionally solidified, suggest that the pore radius ($r_p$) can be considered equal to the size of the dendritic cell, that is:

$$r_p = \frac{\lambda_1}{2} \tag{23}$$

However, this consideration is not quite realistic, since the pore is formed between the dendrites, which present a certain solidified thickness, and therefore the pore will have smaller dimensions than the primary interdendritic spacing. Poirier *et al.* [4], based on a previous study on columnar dendrite microstructures [69], affirmed that the primary arms in general aligned themselves such as adjacent rows and present interlaced rather than square arrangements as showed in Fig. 2b. It is suggested that the radius depends on the geometrical arrangement formed by the dendrites and it also varies with the volumetric fraction of liquid. Supposing that the interlaced arrangement occurs with greater frequency, Poirier *et al.* [4] consider the interdendritic space as being a channel of width $\delta$ and propose that the width of the pore should be determined considering the volumetric fraction of liquid ($g_{liq}$), in the following manner:

$$\delta = \frac{g_{liq}\lambda_1}{2} \tag{24}$$

According to Poirier *et al.* [4] a gas bubble should be inserted into a channel, in which the length ($r_1$) is much larger than the width ($r_2$); when the principal curvature radii are:

$$r_1 = \delta/2 \tag{25}$$

and

$$r_2 \cong \infty \tag{26}$$

and so:

$$r_1 = \frac{g_{liq} \cdot \lambda_1}{4} \tag{27}$$

Kao *et al.* [47] using upward directional solidification, for the Al 4.5 wt% Cu alloy, found an equiaxial grain structure. They assumed that pores nucleate at the root of the dendrites and are controlled by the interdendritic space during the solidification process. They assured that during the last stages of pore growth, the value of $r_2$ is much larger than $r_1$, as shown in Fig. 3. Therefore, the principal curvature radius $r_1$, can be considered as being proportional to the secondary spacing, it is assumed that:

$$r_1 = \frac{\lambda_2}{4} \tag{28}$$

Zou *et al.* [55] modeling the formation of microporosities in A356 alloy with equiaxial grains, also adopt this equation for porosity radius.

There are still models [13], which do not consider the pressure caused by surface tension; this would be a limit case of an infinite pore radius. With this consideration there would be no initial resistance for the gas bubble formation, and the amount of porosities would depend only on the amount of gases present in the alloy. However, this consideration does not agree with experimental results found in literature, where the amount of porosities decreases in cast parts having a refined structure [46].

## 3. Experiment

Fig. 1 shows the experimental setup used for upward directional solidification of the Al 4.5 wt% Cu alloy. The alloy was melted and poured at 1023 K in a cylindrical holder tube, with diameter of 40 and 250 mm in length, made of ceramic material, mounted over a water cooled cooper mould and kept at 973 K. Temperature variations during solidification, in the casting and mold were measured with *chromel-alumel* thermocouples inserted at different positions (Fig. 1), coupled to a data acquisition system. The initial hydrogen content of the melt was determined using a Telegas apparatus [48].

The microstructure was analyzed through optical microscopy. The transverse and longitudinal sections of the samples were polished and attacked with Keller's reagent to measure the primary and secondary dendrite arm spacing. Transversal samples were used to measure the primary dendrite arm spacing and longitudinal samples were used to measure the secondary dendrite arm spacing [24]. Pore fraction was measured by image analysis.

## 4. Results and discussion

Thermophysical properties of the Al 4.5 wt% Cu used in the simulations performed are in Table I. Although the method is applied to aluminum alloys, it is generally valid and can be easily extended to other systems. The temperature variations experimentally monitored were used in a finite difference heat flow program to determine the transient metal/mold heat transfer coefficient. The coefficient varies from about 4,000 to 1,000 W/($m^2$K) during the solidification process [17].

The variations of the interdendritic arm spacings during solidification were determined using the temperature variations, the advance velocities of dendrite tip, the local solidification time and the thermal gradients in front of the dendrite tip, obtained with the numerical model.

Fig. 4 presents microstructures of cross section of samples at 10, 70 and 110 mm from metal/mould interface, showing the primary dendrite arms. Fig. 5 presents microstructures of transversal sections of samples at 20,

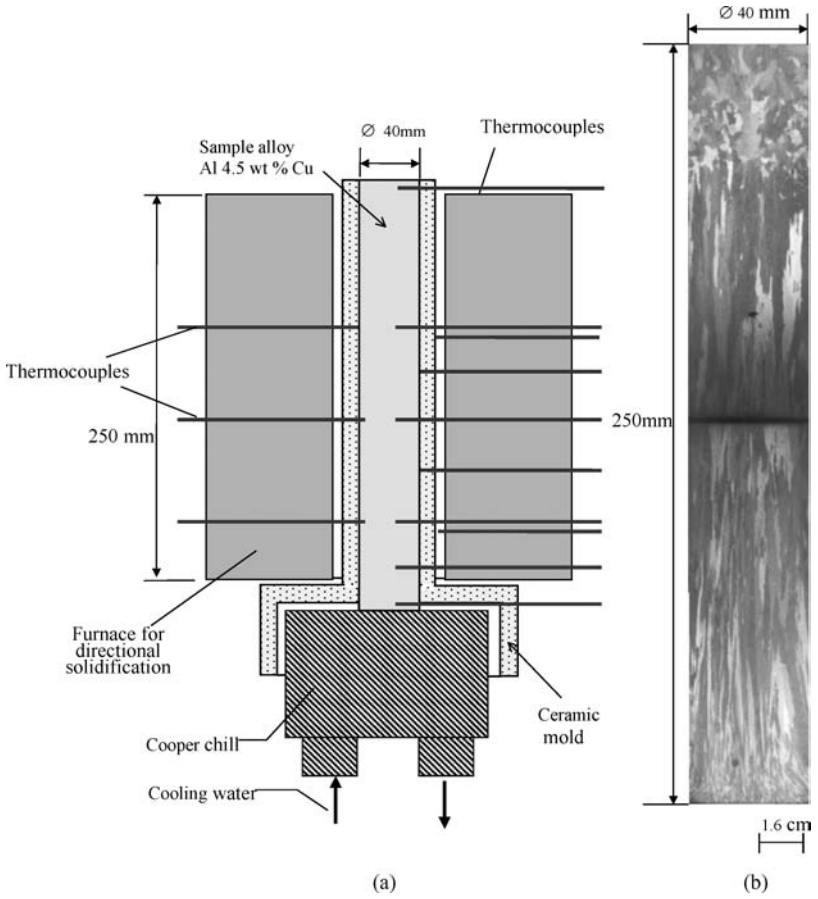


*Figure 1* (a) Schematic illustration of the experimental apparatus used to directionally solidify. (b) Unidirectional macrostructure obtained the Al 4.5 wt% Cu alloy.

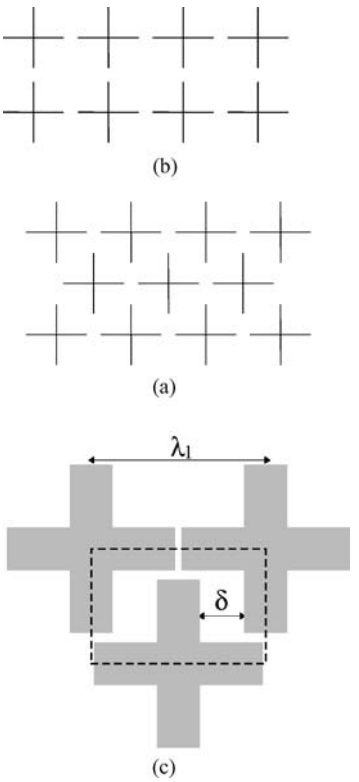


*Figure 2* Schematics presented by Poirier *et al.* [4] of the arrangements of primary dendrite arms (a) interlocking arrangement (b) square arrangement, and (c) dendritic grooves among three primary dendrite arms. Arrangements (a) and (b) presented by Jacobi [69].

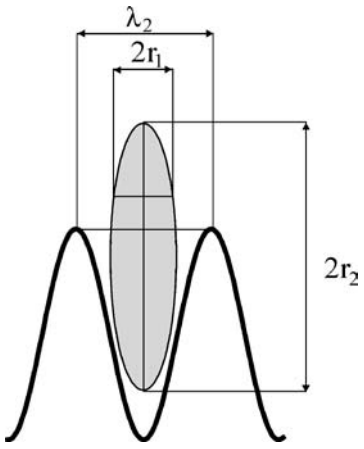


*Figure 3* Schematics presented by Kao *et al.* [47] for pore formation.

35 and 190 mm from metal/mould interface, showing the secondary dendrite arms. It is observed that both primary and secondary dendrite arms spacings increase with the distance from metal/mould interface.

As an example of application of the numerical model, Fig. 6 presents the results obtained for primary dendrite arm spacing ($\lambda_1$) as function of cooling rate, using different theoretical models. The equations for high velocities proposed by Kurz and Fischer [18], Trivedi [23], Geying and Lixin [24] and Hunt [22] are similar, differing only by constants, giving parallel curves. These

TABLE I Constants and thermophysical properties of Al 4.5 wt% Cu Alloy

| Description | Value | Temperature | Reference |
|---|---|---|---|
| Melting temperature base metal | 660.4 (°C) | - | Kurz and Fisher, 1986 [18] |
| Liquid temperature | 646 (°C) | – | Voller and Swaminathan, 1991 [70] |
| Eutectic temperature | 548 (°C) | – | Kubo and Pelhke, 1985 [5] |
| Eutectic composition | 33.2 (%) | 548(°C) | Kubo and Pelhke, 1985 [5] |
| Specific heat | 0.9 (kJ/kgK) 1.1(kJ/kgK) | 548(°C) 645(°C) | Voller and Sundarraj, 1995 [71] |
| Thermal conductivity | 200 (W/mK) 100 (W/mK) | 548(°C) 645(°C) | Voller and Sundarraj, 1995 [71] |
| Latent heat in melting | 385000 (J/kg) | – | Swaminathan and Voller, 1992 [72] |
| Density—solid phase | 2610 (kg/m$^3$) | 548(°C) | Poirier *et al.*, 1987 [63] |
| Density—liquid phase | 2450 (kg/m$^3$) | 652(°C) | Poirier *et al.*, 1987 [63] |
| Interfacial liquid-gas energy | 0.825 (N/m$^2$) | – | Emadi, Gruzleski, Toguri, 1993 [49] |

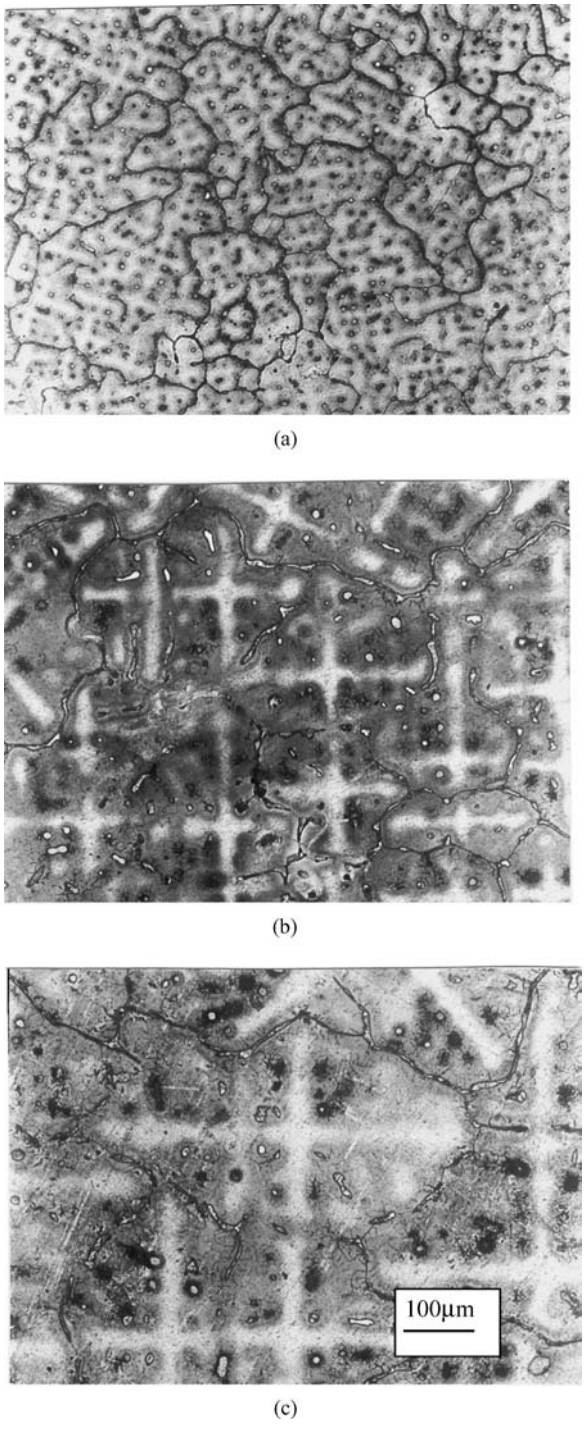


*Figure 4* Micrographs of unidirectionally solidified Al 4.5 wt% Cu alloy, cross section showing the variation in primary interdendric spacings with the distance from the cooled copper chill. Magnification: 100×. Keller attack: (a) Distance from chill 10 mm, (b) Distance from chill 70 mm, and (c) Distance from chill 110 mm.

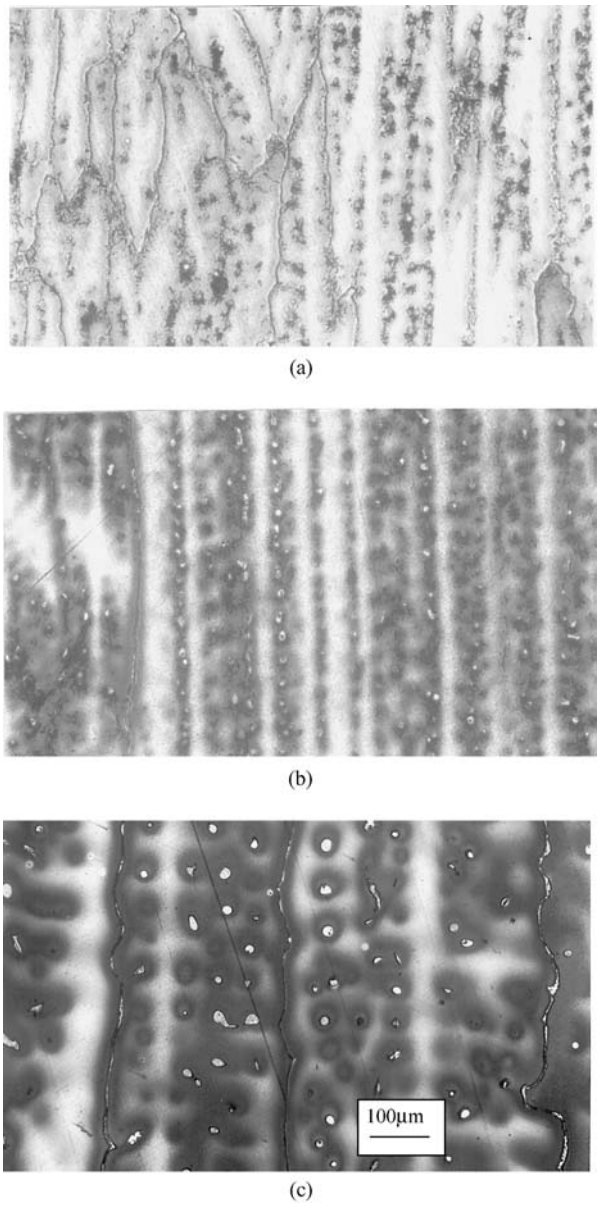


*Figure 5* Micrographs of unidirectionally solidified Al 4.5 wt% Cu alloy, transversal section showing variation in secondary interdendritic spacings with the distance from the cooled copper chill. Magnification: 100×. Keller attack: (a) Distance from chill 20 mm, (b) Distance from chill 35 mm, and (c) Distance from chill 190 mm.

differences result from the geometrical considerations initially assumed by the authors. Fig. 7 presents the experimental results for $\lambda_1$ as function of the distance from metal/mould interface obtained in this work, compared with results obtained with the numerical model

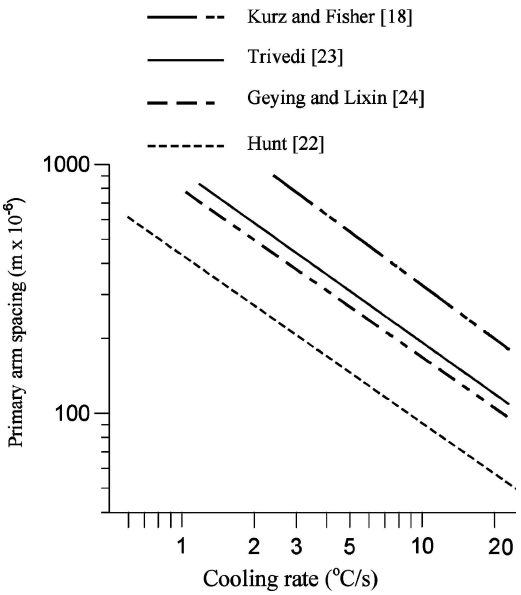


*Figure 6* Predictions of the primary interdendritic spacing of Al 4.5 wt% Cu alloy of different models in literature [18, 22–24] as function of the cooling rate.

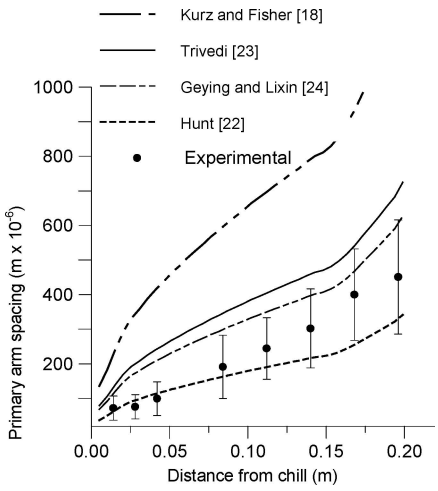


*Figure 7* Variations in primary spacing for different models [18, 20–22] compared to the experimental data for the directionally solidified Al 4.5 wt% Cu alloy.

using the cited equations [18, 22–24]. It can be seen that the Hunt model [22] describes satisfactorily the variation of primary spacing, specially for high cooling rates. The other models present the same growth tendency, but dislocated upwards. The empirical models proposed for primary spacing [25, 32] were also tested but the results obtained did not described satisfactorily the experimental observation.

Fig. 8 presents the comparison between the experimental results for secondary arm spacing as function of the distance from metal/mould interface obtained in this work with those obtained by the numerical model using models proposed by different authors [28–30, 34]. Analyzing Fig. 8 it is observed that the empirical models proposed by Bower [30] and Jones [34] fit well with the experimental results. The theoretical models by Feurer [28] and Kirkwood [29] present the same tendency, however, dislocated upwards. It must be emphasized that the models are not necessarily incorrect, but inadequate for the solidification conditions observed in this work.

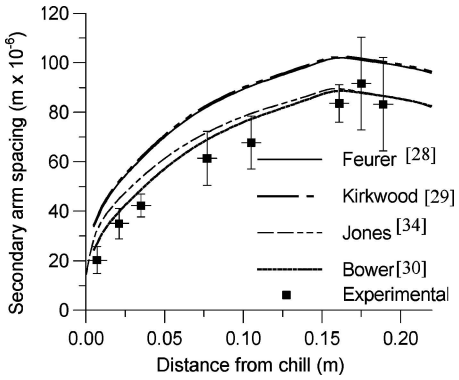


*Figure 8* Variations in secondary spacing for different models Bower [28] and Jones [32] Feurer [26] and Kirkwood [27] compared to the experimental data for the directionally solidified Al 4.5 wt% Cu alloy.

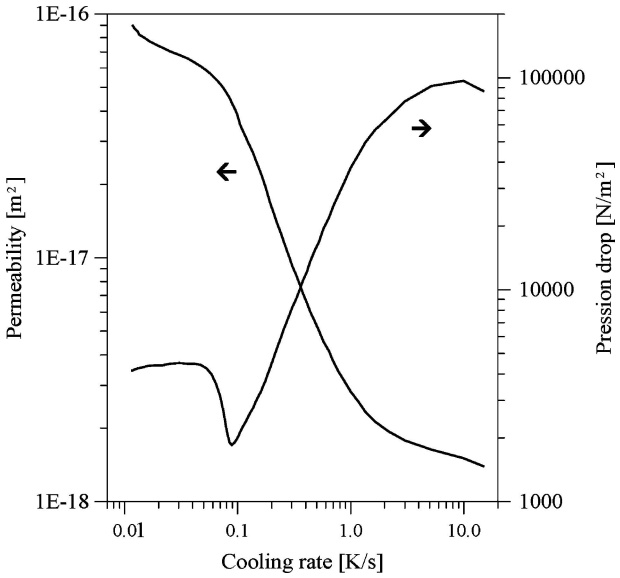


*Figure 9* Permeability and pressure drop variation with cooling rate during Al 4.5 wt% Cu solidification.

During the solidification, continuous variation of primary and secondary arms spacings is observed and the permeability of the interdendritic channels also varies. From equation [20] it is observed that permeability decreases when primary dendrite arms spacing decreases, secondary arms spacing increase and liquid fraction decreases. This variation affects the pressure drop in the interdendritic channels during the liquid flow.

Fig. 9 shows the variation of pressure drop and permeability with cooling rate obtained by the numerical model applying the Hunt and the Bower models, respectively, to calculate variations of primary and secondary dendrite arms spacings. It is observed that permeability increases when the cooling rate decreases, and the pressure drop initially decreases as permeability increases, as expected. But when the cooling rate that decreases during solidification, reaches a certain value affecting the extension of the mushy zone and the rate of the *solidus* isotherm movement, the pressure drop increases, despite the increase in permeability.

In the case of the upward directional solidification of the Al 4.5 wt% Cu alloy, it is observed a formation

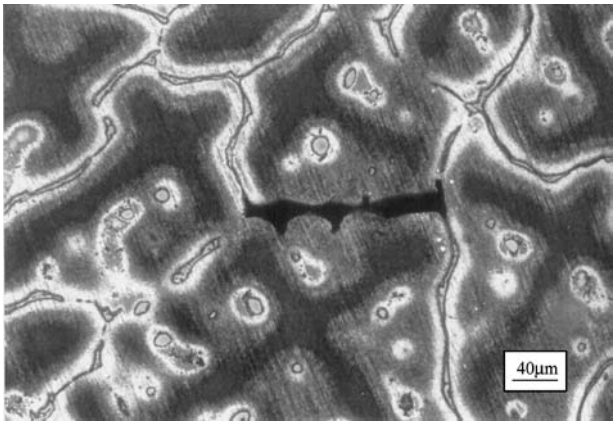


*Figure 10* Microphotography of the Al 4.5 wt% Cu alloy transverse section at a distance of 110 mm from the metal/chill mold interface. Magnification: 250×.

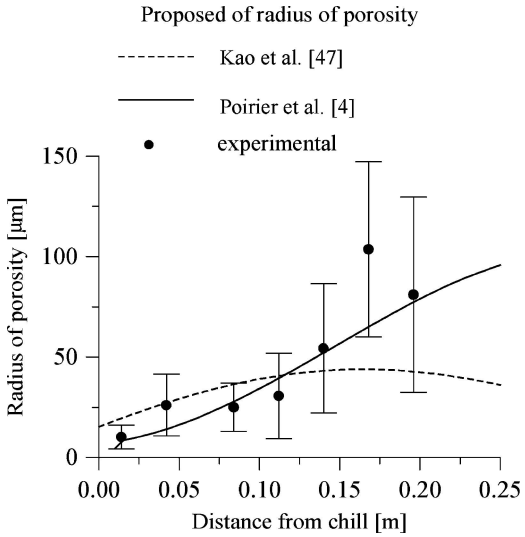


*Figure 11* Variations in the porosity radius predicted by the numeric model, assuming different proposals for the porosity radius, compared to the experimental results obtained from the directionally solidified Al 4.5 wt% Cu alloy.

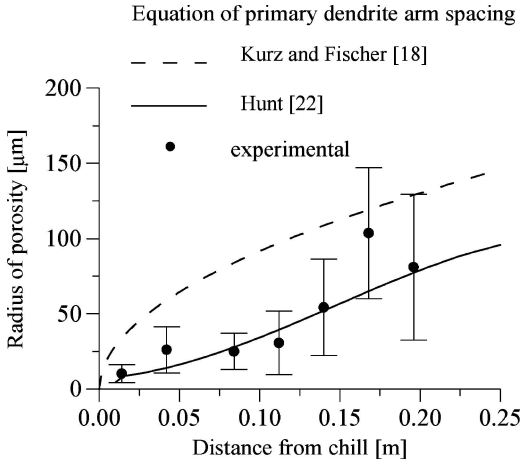


*Figure 12* Variations in the porosity radius predicted by the numeric model, assuming different models for the primary interdendritic spacing, compared to the experimental results obtained from the directionally solidified Al 4.5 wt%Cu alloy.

of columnar structure in almost the entire sample. The interdendritic feeding is strongly favored, as the primary arm spacing only increases with the distance from the chill mold, leading to a increase in the permeability during solidification. Lee *et al.* [46], considering similar results with an Al 7 wt% Si-0.3 wt% Mg alloy affirm that the pressure drop diminishes due to the high permeability of the coarse structure which facilitates interdendritic feeding. Sigworth and Wang [7–9] affirm that the drop in pressure, in the presence of gases, does not exert influence on the formation of pores in aluminum alloys, as the order of magnitude is much smaller than that of the gas pressure. Analyzing the experimental results obtained as, for example, those presented in Fig. 10, it is possible to observe the occurrence of microporosity in most of the extension of the sample, increasing with the distance from metal/mould interface. This occurs because it is observed a significant increase in the primary spacing for low cooling rates, as illustrated in Figs 4, 6 and 7, and the pressure due to surface tension ($P_\sigma$) decreases, as indicated in Equation 21, offering low resistance to the formation of microporosities by dissolved gases. As the metalostatic pressure ($P_M$), in the case of aluminum alloys, is relatively small, the gas pressure ($P_G$) has to overcome only the atmospheric pressure ($P_A$). Another reason for this increase in microporosities is that the solidification rate decreases with the distance from metal/mould interface giving more time for hydrogen to diffuse to the bubbles already formed.

Fig. 11 presents the results of pore radius as function of distance from metal/mould interface obtained applying models proposed for two distinct conditions: assuming that the microporosities are (1) interdendritic, adopting the Poirier *et al.* [4] proposal and (2) intradendritic, adopting the suggestion of Kao *et al.* [47] and Zou *et al.* [55], compared with the experimental results for the directionally solidified Al 4.5 wt%Cu alloy. These results were obtained considering an initial hydrogen content of 0.10 cc/100 g Al. Analyzing Fig. 11, it is seen that the results of the model for interdendritic microporosities agrees better with the experimental results. As seen in Fig. 10, interdendritic microporosities were found in the directionally solidified Al-4.5 wt% Cu alloy between the columnar dendrites, confirming these results. The space between primary branches is much larger than the space between the secondary branches, therefore the pressure needed to form a gas bubble is much smaller between primary branches than between secondary branches [4]. So, the adoption of intradendritic microporosities, when in truth they are interdendritic, results in an underestimated profile for their dimensions.

Fig. 12 presents the results of the numerical model, assuming that the microporosities are interdendritic [4], but using two models to predict the primary interdendritic spacing, Kurz and Fischer [18] and Hunt [22], compared with the experimental results for the porosity radii in the directionally solidified Al 4.5 wt% Cu alloy, for an initial hydrogen content of 0.10 cc/100 g Al. Analyzing Fig. 12, one notes that adopting an inadequate model to predict microstructure can cause great discrepancies in the results of the predicted dimensions for the microporosities.

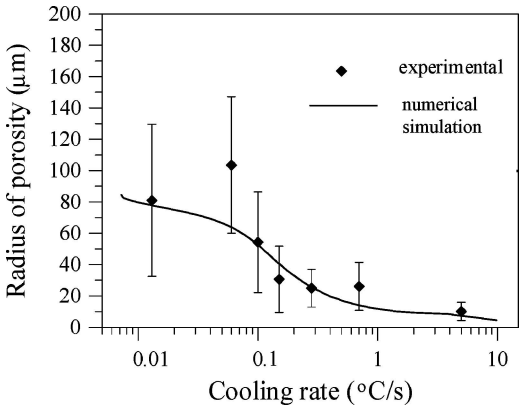


*Figure 13* Variations in the porosity radius predicted by the numeric model, compared to the experimental results obtained from the directionally solidified Al 4.5 wt%Cu alloy, as function the cooling rate.

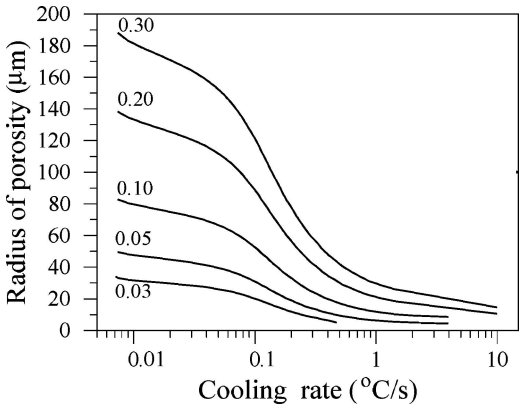


*Figure 14* Pore radius variation considering the cooling rate for different initial hydrogen concentrations as the cooling rate function.

Fig. 13 presents the variation in pore radius as function of the cooling rate, predicted by the numerical model compared to the equivalent mean radius measured in the samples also for an initial hydrogen content of 0.10 cc/100 g Al. It can be observed that the porosity dimensions increase with the decrease in the rate. These results are similar to those found by Emadi and Gruzleski [49] for the A356 alloy (modified or not), which observed that the volumetric fraction and the dimensions of microporosities increase with the decrease in rate, and this increase is more abrupt for low cooling rates, below 1°C/s.

Fig. 14 presents the variations in pore radii, estimated by the numerical model, as function of the cooling rate, for different initial hydrogen concentrations. It can be seen that, for the same thermal conditions and for the same alloy, pore radius increases with the increasing initial hydrogen content. This occurs due to the fact that the gas pressure ($P_G$) exceeds the acting pressure much more easily with the increase in hydrogen concentration. It can also be noted that the formation of porosities can be avoided for certain hydrogen contents by increasing the cooling rate.

## 5. Conclusions

Numerical and experimental results presented in this paper indicate that the numerical model permits a sufficiently precise analysis of the formation of microporosity by dissolved gases and by shrinkage of metallic alloys during solidification, considering interdendritic spacing and porosity radius, initial hydrogen content and the thermal conditions of the process. The pressure drop in the interdendritic channels is affected by permeability of the channels, cooling rate, extension of the mushy zone and rate of *solidus* isotherm movement.

From the results obtained it is possible to conclude that for cooling rates above 1°C/s the possibility of pore formation increases, affected by smaller primary and secondary interdendritic arms spacing, that decreases the permeability and increases pressure drop.

To predict the formation of microporosity, it is necessary to determine which is the more convenient equation to estimate the primary and secondary interdendritic arm spacing, for the alloy and thermal conditions applied. In the case of upward directional solidification of the Al 4.5 wt% Cu alloy, it was observed that the equations which best describe the primary and secondary spacing are the Hunt and Bower respectively.

For the case of the upward directional solidification of the Al 4.5 wt% Cu alloy, in which a columnar structure was formed in almost the entire extension of the sample, the pressure drop is always less than the acting pressure, indicating that there is no pore formation due to shrinkage and that the pores formed are related to the presence of gases.

Adoption of the proper equation for the initial microporosity radius is decisive in the precision of the model, as it directly influences the pressure caused by surface tension, which makes difficult the bubbles formation.

For a certain cooling rate the volumetric pore fraction and the size of the pores increase with the initial hydrogen content. This is more significant for smaller cooling rates.

Diminishing the cooling rate (below 1°C/s), the formation of microporosities by gases is favored, since the larger the interdendritic spacing the smaller will be the pressure due to surface tension, which difficult pore nucleation.

## Acknowledgements

The authors acknowledge the financial support provided by CNPq (The Brazilian Research Council) and FAPESP (The Scientific Research Foundation of State of São Paulo).

## References

1. T. S. PIWONKA and M. C. FLEMINGS, *Trans. TMS-AIME* **236** (1966) 1157.
2. J. CAMPBELL, "Castings" (Butterworh-Heinemann, Oxford, 1991).
3. T. OKAMOTO and K. KISHITARE, *J. Cryst. Growth* **29** (1975) 137.
4. D. R. POIRIER, K. YEUM and A. L. MAPLES, *Metall. Trans. A* **18** (1987) 1979.
5. K. KUBO and R. D. PEHLKE, *ibid. B* **16** (1985) 359.
6. D. ARGO and J. E. GRUZLESKI, *AFS Trans.* **96** (1989) 67.
7. G. K. SIGWORTH and C. WANG, *Am. Foundrymen's Soc. Trans.* **100** (1992) 979.
8. *Idem.*, *Metall. Trans. B* **24** (1993) 349.
9. G. K. SIGWORTH, C. WANG, H. HUANG and J. T. BERRY, *Am. Foundrymen's Soc. Trans.* **102** (1994) 245.

10. G. K. SIGWORTH and T. A. ENGH, *Metall. Trans. B* **13** (1982) 447.
11. K. YEUM and D. R. POIRIER, " Light Metals, Warrendale," PA (1988) 469.
12. X. G. CHEN and S. ENGLER, *AFS Trans.* **102** (1994) 673.
13. A. V. KUZNETSOV and K. VAFAI, *Int. J. Mass Trans.* **38** (1995) 2557.
14. N. ROY, A. SAMUEL and F. H. SAMUEL, *Metall. Trans. A* **27** (1996) 415.
15. M. L. N. M. MELO, E. M. S. RIZZO and R. G. SANTOS, *Mater. Sci. Forum* **242** (1997) 83.
16. CH. PEQUET, M. GREMAUD and RAPPAZ, *Metall. Trans. A* **33** (2002) 2095.
17. M. L. N. M. MELO, E. M. S. RIZZO and *R. G. SANTOS, Mater. Sci. Eng. A* **374** (2004) 351.
18. W. KURZ and D. J. FISHER,"Fundamentals of Solidification" (Trans Tech Publications, Aedermannsdorf, 1992).
19. K. A. JACKSON and J. D. HUNT, *Trans. TMS-AIME* **236** (1966) 1129.
20. M. RAPPAZ and D. M. STEFANESCU, " Metals Handbook", (ASM, Ohio, USA, 1988) Vol. 15, p. 883.
21. E. SCHEIL, *Zeitschrift fur Metallkunde* **34** (1942) 70.
22. J. D. HUNT, "Solidification and Casting of Metals" (The Metals Society, London, 1979).
23. R. TRIVEDI, *Metall. Trans. A* **15** (1984) 977.
24. A. GEYING and L. LIXIN, *J. Crystal Growth* **80** (1987) 383.
25. K. P. YOUNG and D. H. KIRKWOOD, *Metall. Trans. A* **6** (1975) 197.
26. M. C. FLEMINGS, "Solidification Processing" (McGraw-Hill, New York, 1974) p. 234.
27. G. B. SALAS, J. V. RAMÍREZ, A. M. E. NOGUEZ and T. N. ROBERT, *Scrip. Metall. et Mater.* **32** (1995) 295.
28. U. FEURER, in Proceedings of The Symposium on Quality Control of Engineering Alloys (Delft, 1977) p. 131.
29. D. H. KIRKWOOD, *Mater. Sci. Eng.* **73** (1985) L1.
30. T. F. BOWER, H. D. BRODY and M. C. FLEMINGS, *Trans. AIME* **236** (1966) 624.
31. S. H. HAN and R. TRIVEDI, *Acta Metall. Mater.* **42** (1994) 25.
32. D. G. McCARTNEY and J. D. HUNT, *Acta Metall.* **29** (1981) 1851.
33. J. D. HUNT and S. Z. LU, *Metall. Trans. A* **27** (1996) 611.
34. R. C. PRATT, H. JONES and G. J. DAVIES, in Proceedings of the Solidification Processing (Sheffield, UK, 1987) p. 349.
35. R. A. PRATT and R. N. GRUEL, *Mater. Charac.* **31** (1993) 225.
36. D. H. BRODY and M. C. FLEMINGS, *Trans. TMS-AIME* **236** (1966) 615.
37. T. W. CLYNE and W. KURZ, *Metall. Trans. A* **12** (1981) 965.
38. D. R. POIRIER, *B ibid.* **18** (1987) 245.
39. R. MEHRABIAN, M. KEANE and M. C. FLEMINGS, *ibid.* **1** (1970) 1209.
40. D. APELIAN, M. C. FLEMINGS and R. MEHRABIAN, *ibid.* **5** (1974) 2533.
41. N. STREAT and F. WEINBERG, *ibid.* **7** (1976) 417.
42. O. NIELSEN and L. ARNBERG, *ibid.* **31A** (2000) 3149.
43. B. GOYEAU, MT. BENIHADDADEBE, D.GOBIN and M. QUINTARD, *ibid. B* **30** (1999) 613.
44. P. ROUSSET, M. RAPPAZ and B. HANNART, *ibid. A* **26** (1995) 2349.
45. P. D. LEE, A. CHIRAZI and D. SEE, *J. Light Met.* **1** (2001) 15.
46. Y. W. LEE, E. CHANG and C. F. CHIEU, *Metall. Trans. B* **21** (1990) 715.
47. S. T. KAO, E. CHANG and Y. W. LEE, *Mater. Sci. Tech.* **11** (1995) 933.
48. G. LASLAZ and P. LATY, *AFS Trans.* **99** (1991) 83.
49. D. EMADI, J. E. GRUZLESKI and J. M. TOGURI, *Metall. Trans. B* **24** (1993) 1055.
50. W. S. PELLINI, *Trans. Amer. Foundr. Soc.* **61** (1953) 61.
51. S. MINAKAWA, I. V. SAMARASKERA and F. WEINBERG, *Metall. Trans. B* **16** (1985) 823.
52. J. LECOMTE-BECKERS, *ibid. A* **19** (1988) 2342.
53. I. J. CHIOU and H. L. TSAI, *AFS Trans.* **98** (1990) 823.
54. Q. T. FANG and D. A. GRANGER, *ibid.* **97** (1989) 989.
55. J. ZOU, S. SHIVKUMAR and D. APELIAN, *ibid.* **98** (1990) 872.
56. W. LA ORCHAN and J. E. GRUZLESKI, *ibid.* **100** (1992) 415.
57. J. AMPUERO, A. HOADLEY and M. RAPPAZ, in Proceedings of 5th Modeling of Casting, Welding and Advanced Solidification Process, Warrendale (1991) p. 449.
58. Q. HAN and S. VISWANATHAN, *Metall and Trans.* **A33** (2002) 2067.
59. W. R. OPIE and N. J. GRANT, *Trans. AIME* 188 (1950) 1241.
60. D. E. J. TALBOT, *Int. Metall. Reviews* **20** (1975) 861.
61. P. C. CARMAN, *Trans. Inst. Chem. Eng.* **14** (1937) 150.
62. D. A. NIELD and A. BEJAN, "Convection in Porous Media" (Springer-Verlag, New York, 1992).
63. D. R. POIRIER and K. YEUM, in Proceedings of the Solidification Processing, Sheffield, England (1987) p. 26.
64. S. M. BOUNDS, G. J. MORAN, K. A. PERICLEOUS and M. CROSS, in Proceedings of the 8th Modeling of Casting, Welding and Advanced Solidification Processes, edited by B. G. Thomas e C. Beckermann (TMS, 1998) p. 171.
65. R. G. SANTOS and M. LN. M. MELO, in Proceedings of 3rd Joint of Group of Computational Mechanics and Ibero-Latin American Association of Computational Methods in Engineering, Giullanova, Italy (2002) CDROM.
66. K. MURAKAMI, A. SHIRAISHI and T. OKAMOTO, *Acta Metall.* **32** (1984) 1423.
67. A. K. GUPTA, B. K. SAXEMA, S. N. TIWARI and S. L. MALHOTRA, *J. Mater. Sci.* **27** (1992) 853.
68. D. R. POIRIER and R. SPEISER, *Metall. Trans.* **A18** (1987) 1156.
69. H. JACOBI, "Crystallization of Steel in Information Symposium, Casting and Solidification of Steel" (IPC Science and Technology Press Ltd., England, 1977) Vol. 1, p. 111.
70. V. R. VOLLER and C. R. SWAMINATHAN, *Numer. Heat Trans., Part B* **19** (1991) 175.
71. V. R. VOLLER and S. SUNDARRAJ, *Int. J. Heat Mass Trans.* **38** (1995) 1009.
72. C. R. SWAMINATHAN and V. R. VOLLER, *Metall. Trans. B* **23** (1992) 651.

*Received 30 March*
*and accepted 6 December 2004*